Short-range longitudinal wake function of undulator lines at the European x-ray free electron laser

Igor Zagorodnov*, Martin Dohlus, Torsten Wohlenberg

Deutsches Elektronen-Synchrotron DESY, Notkestr. 85, 22607 Hamburg, Germany

Abstract

We derive an analytical approximation of the short-range longitudinal wake function of undulator lines at the European x-ray free electron laser. The used analytical and numerical approaches are described. A numerical algorithm to estimate the impedance of arbitrary shaped pipes with known surface impedance is presented. We discuss a choice of the optimal linear undulator taper for a known wake function.

Keywords: free electron laser, electromagnetic fields, numerical methods, wake fields

1. Introduction

The numerical modeling of modern x-ray free electron lasers (XFEL's) remains a challenge due to different scales in time and space of the physical processes involved. The impact of the properties of the vacuum chamber on the electron beam can be taken into account in the numerical modeling by wake field formalism [1]. It means that the fields of the electron beam scattered by the vacuum chamber are precalculated and their impact on the particles in the beam is described by wake potential. In this paper we are interested only in the longitudinal component of the wake potential which is defined by the expression

$$W_{\parallel}(s) = -\frac{1}{Q}\int_{-\infty}^{\infty} E_z\left(z, t = \frac{z+s}{c}\right) dz, \tag{1}$$

*Corresponding author
Email address: Igor.Zagorodnov@desy.de (Igor Zagorodnov)

where E_z is the longitudinal component of the electric field on the reference trajectory, Q is the bunch charge, c is the light velocity in vacuum, s is the longitudinal position of the test particle in the bunch.

In order to avoid the numerically time-consuming and tedious process of calculation of the wake potential for different bunch shapes with electromagnetic codes it is desirable to have an estimation of the longitudinal wake function $w_{\parallel}(s)$ which describes the impact of the point charge alone. If the longitudinal wake function $w_{\parallel}(s)$ is known then the longitudinal wake potential for an arbitrary linear charge density $\lambda(s)$ can be found by convolution

$$W_{\parallel}(s) = -\int_{-\infty}^{s} w_{\parallel}(s - s')\lambda(s')ds'. \tag{2}$$

In this paper we derive an analytical approximation of the short-range longitudinal wake function of undulator lines at the European XFEL. The wake functions of different components of the undulator lines are calculated separately and the total wake function is obtained as a direct sum of the individual contributions. The used analytical and numerical approaches are described. A numerical algorithm to estimate the impedance of arbitrary shaped pipes with known surface impedance is presented. Finally, in the last section we discuss a choice of the optimal linear undulator taper for the wake function obtained.

2. Layout of the undulator lines at the European x-ray free electron laser

The European XFEL produces the hard x-rays down to sub-angstrom wavelength. It consists of a 17.5 GeV linear accelerator (linac) and several undulator lines for Self-Amplified Spontaneous Emission (SASE), namely, SASE1, SASE2 and SASE3 [2]. The SASE1 line consists of 35 undulator segments of length $L_u = 5$ m inter-spaced by 1.1 meters intersections with different devices shown in Fig. 1. The SASE2 line has the same layout and the SASE3 line has a similar layout with different undulator parameters and with only 21 segments.

From the point of the wake field calculation we have periodic structures with period $L = 6.1$ m of the same geometry for all three undulator lines. In Table 1 we list all

Table 1: The components of the undulator lines along one section of length of 6.1 m.

N	Name	Half-width	Half-height	Position	Length	Material
		mm	mm	mm	mm	
1	Elliptical gasket	7.525	4.425	0	0.5	Silver
2	Flange, type I	7.5	4.4	0.5	13.0	Steel 316LN
3	Flange, type II	7.5	4.4	13.5	12.55	Aluminum
4	Weldseam	8.1	5	26.05	0.1	Steel 316LN
5	Elliptical pipe	7.5	4.4	26.15	5436.7	Aluminum
6	Weldseam	8.1	5	5462.85	0.1	Steel 316LN
7	Flange, type II	7.5	4.4	5462.95	12.55	Aluminum
8	Flange, type I	7.5	4.4	5475.5	13.0	Steel 316LN
9	Elliptical gasket	7.525	4.425	5488.5	0.5	Silver
10	Flange, type III	7.5	4.4	5489	27.5	Copper
11	Absorber	4.5	4	5516.5	3	Copper
12	Round pipe	5	-	5519.5	22.2	Copper
13	Below gap	12.75	-	5541.7	2.5	Copper
14	Round pipe	5	-	5544.2	96.3	Copper
15	Pumping slots	5	-	5640.5	21	Copper
16	Round pipe	5	-	5661.5	48.5	Copper
17	Round gasket	5.025	-	5710	0.5	Silver
18	BPM	5	-	5710.5	99	Steel 316LN
19	Round gasket	5.025	-	5809.5	0.5	Silver
20	Round pipe	5	-	5810	68.5	Cooper
21	Below gap	12.75	-	5878.5	2.5	Copper
22	Round pipe	5	-	5881	211	Copper
23	Round/elliptical transition	5 to 7	5 to 4.4	6092	8	Copper

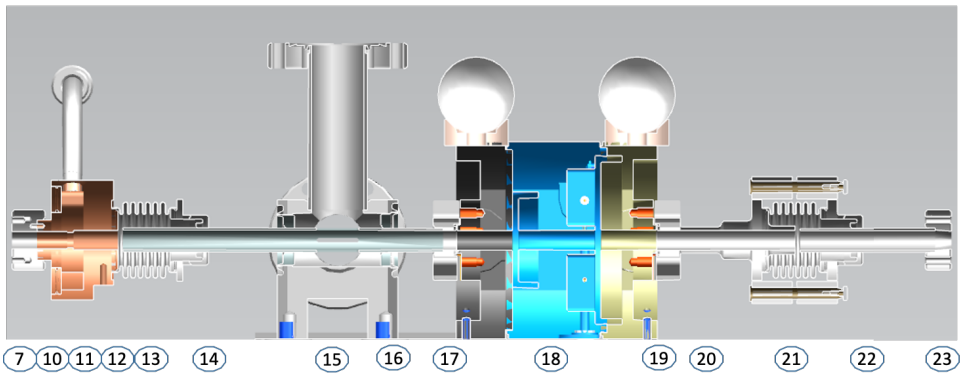

Figure 1: The layout of the undulator intersection. The numbers under the elements correspond to the positions in Table 1.

Table 2: Material properties.

Material	Conductivity $(\Omega m)^{-1}$	Relaxation time fs	Oxide layer nm	Roughness nm
Aluminum	$3.66 \cdot 10^7$	7.1	5	300
Copper	$5.8 \cdot 10^7$	24.6	5	300
Steel 316LN	$1.4 \cdot 10^6$	2.4	0	300
Silver	$6.2 \cdot 10^7$	40	0	300

components which contribute to the wake potentials. Table 2 presents the properties of the materials [3] used in the estimation of the steady-state resistive wall wake fields as described in the following section.

The linac of the European XFEL allows to operate with bunches of arbitrary charge from several picocoulombs up to several nanocoulombs compressed to the peak current of several kiloampers. The longitudinal profiles of the electron bunches can be approximated by a Gaussian shape. In the following we consider as a reference a Gaussian bunch with charge of 250 pC compressed to the peak current of 5 kA. Other parameters of the setup are listed in Table 5. From another side, the wake function obtained in this paper can be used to estimate the wake potentials for arbitrary shaped bunches of arbitrary charge.

3. Wake functions of different components

3.1. Wake functions of round and elliptical pipes

The main contribution to the wake function at the undulator lines is due to the resistive wall wake fields of the elliptical pipe in the undulator segment and the round pipe in the intersection. In order to estimate these contributions we use a steady-state model of the wake fields for the charge moving in an infinitely long pipe of the constant cross-section.

The steady-state longitudinal resistive wall impedance of round pipe with dc conductivity κ_0 and the relaxation time τ can be written as [4]

$$Z_{\parallel}(\omega) = \frac{Z_s}{2\pi a}\left(1 + i\frac{\omega a Z_s}{2cZ_0}\right)^{-1}, \tag{3}$$

where a is the pipe radius, Z_0 is the free space impedance, c is the velocity of light in vacuum and the surface impedance Z_s is given by relations

$$Z_s(\omega) = Z_s^{\kappa}(\omega) = \sqrt{\frac{i\omega Z_0}{c\kappa(\omega)}}, \quad \kappa(\omega) = \frac{\kappa_0}{1 + i\omega\tau}. \tag{4}$$

The effect of the oxide layer and of the roughness can be taken into account through the inductive part of the surface impedance [5, 6]

$$Z_s(\omega) \approx Z_s^{\kappa}(\omega) + i\omega L_s, \quad L_s = \mu_0\left(\frac{\epsilon_r - 1}{\epsilon_r} d_{oxid} + f d_{rough}\right), \tag{5}$$

where d_{oxid} is the depth of the oxide layer, d_{rough} is the rms parameter of the roughness, ϵ_r is a relative dielectric constant of the oxide layer. In the following we suggest that $\epsilon_r = 2$ and $f = 0.01$ [6].

Equations (3)-(5) are used to estimate the contribution of the material properties of the components in the intersection to their wake functions. The contributions due to change of the vacuum chamber geometry are considered in the following sections.

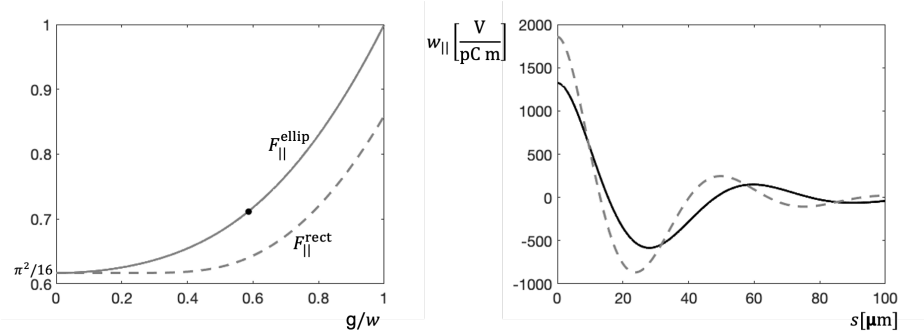

Figure 2: Longitudinal form factors of the elliptical (solid line) and the rectangular (dashed line) pipes are shown in the left plot. The right plot shows the longitudinal wake functions of elliptical (solid black curve) and round (dashed gray curve) aluminum undulator pipes with the same vertical dimensions $2a = 2g = 8.8$ mm.

It is well known [7] that in the origin, $s = 0$, the longitudinal wake function of the parallel plates is by factor $\pi^2/16$ smaller. In order to reduce the strength of the wake fields the pipe in the undulator has not round but an elliptical shape with width $2w = 15$ mm and height $2g = 8.8$ mm (see Fig. 4).

Let us define the longitudinal form factor $F_{||}^{ellip}$ of the elliptical pipe with major semi-axis w and minor semi-axis g as the ratio at the origin of the wake function $w_{||}^{ellip}$ to the wake function of the round pipe $w_{||}^{round}$ of radius g

$$F_{||}^{ellip}\left(\frac{g}{w}\right) = \frac{w_{||}^{ellip}(0)}{w_{||}^{round}(0)}. \tag{6}$$

In the same way we define the longitudinal form factor $F_{||}^{rect}$ of the rectangular pipe with width $2w$ and height $2g$. The analytical expressions of these form factors are derived in Appendix B.

The left plot in Fig. 2 shows the dependence of the form factors from the parameters ratio g/w. The black point in the plot corresponds to the current parameters of the elliptical pipe in the undulator. We see that for very short bunches the used elliptical shape reduces the wake strength by approximately 30%. Even stronger reduction could be reached with the rectangular pipe shape of the same height and width.

There are analytical [8] and numerical [9] approaches to calculate the resistive wall impedance of the elliptical pipe. The analytical method is based on field matching and use of special functions. In the following we calculate the impedance numerically using method of auxiliary sources [10]. The code based on this numerical technique allows to calculate the steady-state wake function for arbitrary cross-section of the pipe. Our equations and the approach are different from those presented in [9]. Let us describe shortly our numerical method and the obtained results.

The charge of relativistic bunch in the frequency domain reads $\rho(x,y)e^{i(\omega t-kz)}$, $\omega = kc$, where z is the longitudinal coordinate, k is the wave number. Due to the linearity of the Maxwell equations all other quantities of interest will have the same form. Hence the Maxwell equations in the frequency domain can be reduced to the second order differential equations for the transverse components of the electromagnetic field, $\boldsymbol{E}_\perp = (E_x, E_y)^T$, $\boldsymbol{H}_\perp = (H_x, H_y)^T$, in the pipe cross-section S:

$$\Delta_\perp \boldsymbol{E}_\perp = \epsilon_0^{-1}\boldsymbol{\nabla}_\perp\rho, \quad \Delta_\perp \boldsymbol{H}_\perp = \boldsymbol{0}, \tag{7}$$

where ϵ_0 is the permittivity of the vacuum and the transverse operators are defined by expressions $\Delta_\perp = \partial_x^2 + \partial_y^2$, $\boldsymbol{\nabla}_\perp = (\partial_x, \partial_y)^T$. Here symbols ∂_x, ∂_y mean the partial derivatives in the transverse directions.

The longitudinal components of the electromagnetic field can be found through the transverse ones

$$E_z = \frac{1}{ik}\left(\nabla_\perp \boldsymbol{E}_\perp - \frac{\rho}{\epsilon_0}\right), \quad H_z = \frac{1}{ik}\nabla_\perp \boldsymbol{H}_\perp. \tag{8}$$

It is shown in Appendix A that the surface impedance boundary condition in the high-frequency approximation, $k >> 1$, can be a written as

$$E_z = \frac{Z_s}{Z_0}E_n, \quad E_t = 0. \tag{9}$$

Let us present the full electric field $\boldsymbol{E}_\perp$ at the position $\boldsymbol{r} = (x, y)^T$ of the point charge e at the position $(0, 0)^T$ as the sum

$$\boldsymbol{E}_\perp = \boldsymbol{E}^s_\perp + \boldsymbol{E}^0_\perp, \tag{10}$$

where $\boldsymbol{E}^0_\perp = e\boldsymbol{r}(2\pi\epsilon_0 c|\boldsymbol{r}|^2)^{-1}$ is the field of the point charge in the free space and $\boldsymbol{E}^s_\perp$ is the field scattered from the surface of the pipe. The components of the scattered field fulfill the boudary value problem for Laplace equation

$$\Delta_\perp \boldsymbol{E}^s_\perp = 0, \quad \boldsymbol{r} \in S, \tag{11}$$

with the boundary conditions

$$\frac{1}{ik}\nabla_\perp \boldsymbol{E}^s_\perp + \frac{Z_s}{Z_0}\boldsymbol{n}\boldsymbol{E}^s_\perp = -\frac{Z_s}{Z_0}\boldsymbol{n}\boldsymbol{E}^0_\perp, \quad \boldsymbol{\tau}\boldsymbol{E}^s_\perp = -\boldsymbol{\tau}\boldsymbol{E}^0_\perp, \quad \boldsymbol{r} \in \partial S, \tag{12}$$

where $\boldsymbol{\tau} = (-n_y, n_x)^T$ is the tangential vector to the pipe contour ∂S and we have used the relations $E^s_z = (ik)^{-1}\nabla_\perp \boldsymbol{E}^s_\perp$, $E^0_z = 0$ in the boundary conditions given by Eq. (9).

Let us introduce an integral operator A of a simple layer

$$[Af](\boldsymbol{r}) = 2\pi \int_{\partial S'} G(\boldsymbol{r} - \boldsymbol{r}')f(\boldsymbol{r}')ds(\boldsymbol{r}'), \quad \boldsymbol{r} \in S, \tag{13}$$

where the contour $\partial S'$ is a contour similar to the pipe contour ∂S but shifted outside by some "small" distance δ. Here $G(\boldsymbol{r}) = (2\pi)^{-1}\log(|\boldsymbol{r}|)$ is the Green function of the two dimensional Laplace operator and we use the shifted contour $\partial S'$ in order to simplify the numerical scheme and to avoid approximation of singular and hyper-singular integrals.

We present the transverse components of the electric field E^s_x and E^s_y in form of the simple layer, Eq. (13), with unknown densities q_x and q_y, correspondingly. Then the boundary condition, Eq. (12), can be rewritten as a boundary integral equation on pipe boundary ∂S with unknown densities q_x and q_y on the auxiliary contour $\partial S'$

$$\begin{pmatrix} \partial_x A + \alpha n_x A & \partial_y A + \alpha n_y A \\ -n_y A & n_x A \end{pmatrix} \begin{pmatrix} q_x \\ q_y \end{pmatrix} = \begin{pmatrix} -\alpha(n_x E^0_x + n_y E^0_y) \\ n_y E^0_x - n_x E^0_y \end{pmatrix}, \quad \alpha = ik\frac{Z_s}{Z_0}, \tag{14}$$

where the integral operator $\partial_x A$ is defined as

$$[\partial_x Af](\boldsymbol{r}) = \int_{\partial S'} \frac{x - x'}{|\boldsymbol{r} - \boldsymbol{r}'|^2} f(\boldsymbol{r}')ds(\boldsymbol{r}'), \quad \boldsymbol{r} \in S. \tag{15}$$

and the integral operator $\partial_y A$ has a similar form.

In order to find the densities q_x and q_y we approximate contour $\partial S'$ by N linear segments of length $h \approx \delta$ and suggest that the densities are constant on each such segment. On the boundary ∂S we assign N equally spaced collocation points. The obtained matrix equation is solved by direct or iterative method.

If the charge densities q_x and q_y are known then the longitudinal impedance can be found from the longitudinal electric field

$$Z_{\|}(\omega) = \frac{-E_z(\mathbf{0})}{ec}, \quad E_z(\boldsymbol{r}) = \frac{1}{ik}\Big([\partial_x A q_x](\boldsymbol{r}) + [\partial_y A q_y](\boldsymbol{r})\Big), \quad r \in S. \tag{16}$$

Eq. (16) is used for the high-frequency part of the impedance above $\omega > 0.1\omega_0$, where $\omega_0 = c(Z_0\kappa_0 g^{-2})^{1/3}$ is a critical frequency of the round pipe of radius g [11]. In order to restore the low-frequency part of the impedance we apply a simple interpolation $Z_{\|}(\omega) = Z_{\|}(\omega_0)\sqrt{\omega/\omega_0}$.

The numerical code is used to estimate the contribution of the material properties of the components of the elliptical shape in the undulator and the intersection as listed in Table 1. In the calculations we used the following parameters: $N = 100$, $\delta = |\partial S|/N$.

Fig. 2 shows the comparison of the wake functions of round and elliptical pipes with material properties of aluminum from Table 2. The round pipe has radius $a = 4.4$ mm and the elliptical pipe has dimensions $g = 4.4$ mm, $w = 7.5$ mm. The relative error of the numerical solution in comparison with the analytical one for the round pipe is 0.1% in L_2-norm and we expect the same level of accuracy for the numerical solution for the elliptical pipe.

From the wake functions calculated numerically for the elliptical pipe shape and analytically for the round pipe shape we estimate the loss factor $k_{\|}$ and the correlated energy spread $k_{\|,rms}$:

$$k_{\|} = -\int_{-\infty}^{\infty} W_{\|}(s)\lambda(s)ds, \quad k_{\|,rms} = \left(\int_{-\infty}^{\infty}(W_{\|}(s) - k_{\|})^2\lambda(s)ds\right)^{1/2}. \tag{17}$$

These contributions are summarized in the impedance budget presented in Table 4.

3.2. Wake functions of geometric transitions between elliptical and round pipes

The main pipe in the undulator section has an elliptical shape with width $2w = 15$ mm and height $2g = 8.8$ mm. The pipe in the undulator intersection is round

with radius $a = 5$ mm. Between the elliptical-to-round transition there is an elliptical absorber with width $2w_a = 9$ mm and height $2g_a = 8$ mm as it is shown in Fig. 3 on the left. The absorber has length of 3 mm. The another transition from the round pipe to the elliptical one is tapered with the taper of length of 8 mm as it is shown in Fig. 3 on the right.

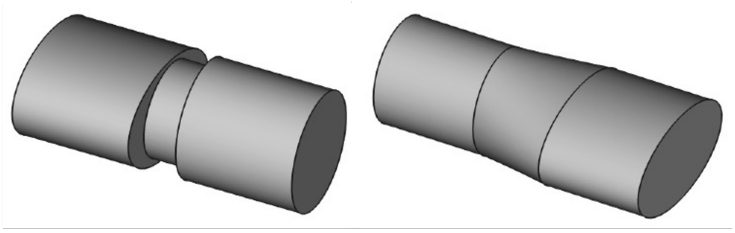

Figure 3: The geometry of transitions between the elliptical and the round pipes. The left picture shows the elliptical-to-round transition with the absorber. The right picture presents the round-to-elliptical transition with the taper.

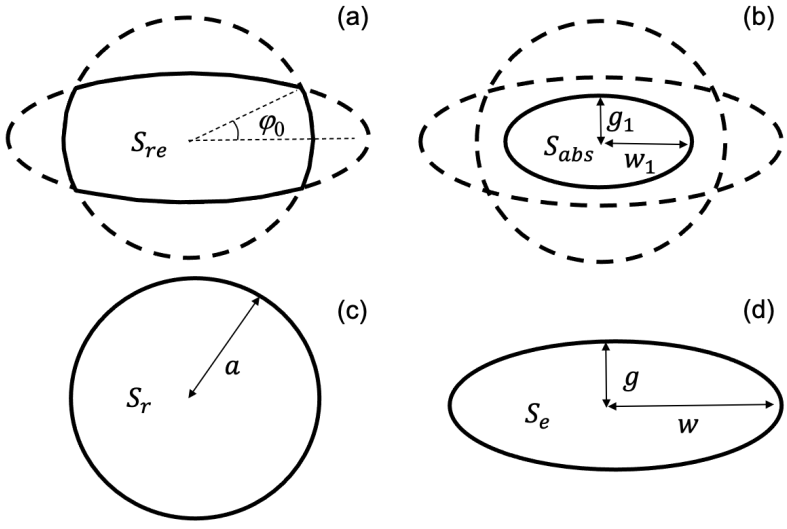

Figure 4: The geometry of transitions between the elliptical and the round pipes. The solid black lines in picture (a) and picture (b) present the integration path for Eq.(18) and Eq.(23). Pictures (c) and (d) show the geometry of elliptical and round pipes shown by dashed lines in pictures (a) and (b) as well.

At the beginning we consider the round-to-elliptical pipe transition, Fig. 4.a. The

bunch of charge of 250 pC compressed to the peak current of 5 kA has a short rms length $\sigma = 5.98\ \mu$m. The transition length $L_{tr} = 8$ mm between the ingoing pipe aperture S_r and the outgoing pipe aperture S_e is short, $L_{tr} << g^2/\sigma$. Hence we are in the optical regime and the high frequency longitudinal impedance is a constant which can be calculated by relation [12]

$$Z_{\parallel}^{re} = \frac{2\epsilon_0}{c}\int_{\partial S_{re}} \phi_e(\mathbf{0},\mathbf{r})\partial_{\mathbf{n}}\phi_r(\mathbf{0},\mathbf{r})dl, \tag{18}$$

where $\mathbf{n}$ is the outward pointing unit normal to the line element dl, and the Green functions for the Laplacian in the pipe cross-sections S_r, S_e read [13]

$$\phi_r(\mathbf{r_0},\mathbf{r}) = \frac{1}{4\pi\epsilon_0}\ln\frac{(x_0y - xy_0)^2 + (xx_0 + yy_0 - a^2)^2}{a^2|\boldsymbol{r} - \boldsymbol{r_0}|^2}, \tag{19}$$

$$\phi_e(\mathbf{r_0},\mathbf{r}) = \phi_e^0(\mathbf{r_0},\mathbf{r}) - \phi_e^0(\mathbf{r_0},(w,0)^T), \tag{20}$$

$$\phi_e^0(\mathbf{r_0},\mathbf{r}) = \frac{1}{\pi\epsilon_0}\sum_{n=1}^{\infty}\frac{e^{-nu}}{n}\left(\frac{\mathrm{Re}T_n(\frac{x+iy}{d})\mathrm{Re}T_n(\frac{x_0+iy_0}{d})}{\cosh(nu)} + \frac{\mathrm{Im}T_n(\frac{x+iy}{d})\mathrm{Im}T_n(\frac{x_0+iy_0}{d})}{\sinh(nu)}\right) +$$
$$+ \frac{1}{4\pi\epsilon_0}\ln((x-x_0)^2 + (y-y_0)^2),$$
$$d = \sqrt{w^2 - g^2}, \quad u = \coth^{-1}(w/g), \quad \boldsymbol{r} = (x,y)^T.$$

Here ϵ_0 is the permittivity of vacuum, T_i are the Chebyshev polynomials of order i.

In the following we suggest that the reference trajectory is on the symmetry axis with coordinates $\boldsymbol{r_0} = (0,0)^T$. The ellipse intersects the x-axis at the point $(w,0)^T$ and due to Eq. (20) the Green function ϕ_e is equal to zero on the ellipse. Hence Eq. (18) can be reduced to a simple form

$$Z_{\parallel}^{re} = \frac{8\epsilon_0}{c}\int_0^{\varphi_0}\phi_e(\varphi,a)\partial_r\phi_r(\varphi,a)rd\varphi = \frac{4}{c\pi}\int_0^{\varphi_0}\phi_e(\varphi,a)d\varphi, \tag{21}$$

where

$$\varphi_0 = \tan^{-1}\left(\frac{g}{w}\sqrt{\frac{w^2-a^2}{a^2-g^2}}\right), \quad \phi_e(\varphi,a) = \phi_e(\mathbf{0},(\varphi,a)^T), \quad \phi_r(\varphi,a) = \phi_r(\mathbf{0},(\varphi,a)^T),$$

and we have used the relation

$$\partial_r\phi_r(\varphi,a) = -\frac{1}{2\pi\epsilon_0 r}. \tag{22}$$

We evaluate the one dimensional integral, Eq. (21), numerically.

In order to find the longitudinal impedance due to the elliptical-to-round transition with the elliptical absorber included we use the equation

$$Z_{\parallel}^{ear} = -\frac{2\epsilon_0}{c}\int_{\partial S_{abs}} \phi_e(\mathbf{0},\mathbf{r})\partial_{\mathbf{n}}\phi_r(\mathbf{0},\mathbf{r})dl + \frac{2}{c}\left(\phi_e(\mathbf{0},\mathbf{0}) - \phi_r(\mathbf{0},\mathbf{0})\right). \tag{23}$$

To simplify the calculation we have applied the relation between the forward $Z_{\parallel}^{ear}$ and the backward $Z_{\parallel}^{rae}$ longitudinal impedances [14, 15]

$$Z_{\parallel}^{ear}(\omega,\boldsymbol{r_1},\boldsymbol{r_2}) = Z_{\parallel}^{rae}(\omega,\boldsymbol{r_1},\boldsymbol{r_2}) + \frac{2}{c}\left(\phi_e(\boldsymbol{r_1},\boldsymbol{r_2}) - \phi_r(\boldsymbol{r_1},\boldsymbol{r_2})\right). \tag{24}$$

Here $Z_{\parallel}^{rae}$ is the impedance of the elliptical-to-round transition (including the absorber) traveled by the charge particle in the backward direction.

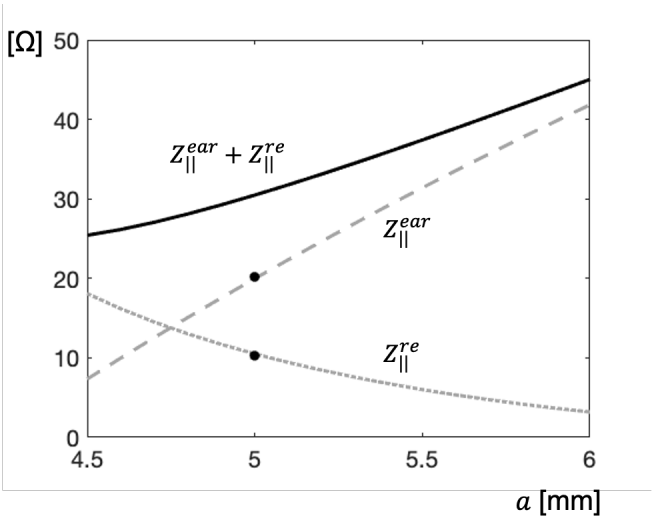

Figure 5: The dependence of impedances $Z_{\parallel}^{re}$ and $Z_{\parallel}^{ear}$ from the round pipe radius a. The black dots show the numerical results calculated by code ECHO [16].

The normal vector $\boldsymbol{n}$ to the ellipse at point (x, y) reads

$$\boldsymbol{n} = (n_x, n_y)^T = \frac{1}{\sqrt{w_1^4 y^2 + g_1^4 x^2}}(g_1^2 x, w_1^2 y)^T. \tag{25}$$

Hence the integral in Eq. (23) in polar coordinates can be written as

$$-\frac{2\epsilon_0}{c}\int_{\partial S_{abs}}\phi_e(\mathbf{0},\mathbf{r})\left(n_x\partial_x\phi_r(\mathbf{0},\mathbf{r})+n_y\partial_y\phi_r(\mathbf{0},\mathbf{r})\right)dl = \\ =\frac{4}{\pi c}\int_0^{\pi/2}\phi_e(\varphi,r)\frac{g_1\cos^2(\varphi)+w_1\sin^2(\varphi)}{r}d\varphi, \tag{26}$$

where $r=\sqrt{w_1^2\cos^2(\varphi)+g_1^2\sin^2(\varphi)}$, and we have used the relations

$$dl=\sqrt{w_1^2\sin^2(\varphi)+g_1^2\cos^2(\varphi)}d\varphi,\quad \partial_x\phi_r(\mathbf{0},\mathbf{r})=-\frac{\cos(\varphi)}{2\pi\epsilon_0 r},\quad \partial_y\phi_r(\mathbf{0},\mathbf{r})=-\frac{\sin(\varphi)}{2\pi\epsilon_0 r}.$$

The dependence of impedances $Z_\parallel^{re}$ and $Z_\parallel^{ear}$ from the round pipe radius a is shown in Fig. 5. The black dots show the numerical results calculated by code ECHO [16] at radius $a=5$ mm. The calculations are done in time domain with the Gaussian bunch of rms length of 12.5 μm. For the round-to-elliptical pipe transition we used a simplified geometry without the taper. The calculated loss factors, $k_\parallel$, can be converted to the impedances by the equation

$$Z_\parallel = 2\sqrt{\pi}\sigma k_\parallel c^{-1}. \tag{27}$$

Table 3: The longitudinal impedances of the pipe transitions in Ohm.

	$Z_\parallel^{re}$	$Z_\parallel^{ear}$
analytical	10.5	20.0
numerical	10.3 (8.3)	20.2

The longitudinal impedances of the transitions are given in Table 3. The numerical results correspond to the black points in Fig. 5. The number in the parentheses is obtained from the code ECHO for the round-to-elliptical transition with the taper included for the bunch with rms length of 12.5 μm. The taper reduces the strength of the wake fields. However, for shorter bunches it will go to the limit given by the analytical estimation in the first row of Table 3. In the impedance budget and in the wake function estimation we will use the analytical values of the first row.

The longitudinal wake functions of the transitions can be written as

$$w_\parallel(s) = cZ_\parallel\delta(s), \tag{28}$$

and the correlated energy spread is given by expression

$$k_{\parallel,rms} = k_{\parallel}\sqrt{\frac{2}{\sqrt{3}} - 1} = 0.4k_{\parallel}.$$

3.3. Wake functions of beam position monitor, vacuum pump, belows and other components

In this section we describe the geometries and the wake functions of the remaining components listed in Table 1: the beam position monitor (BMP), the vacuum pump, the belows, the gaskets and the weldseams.

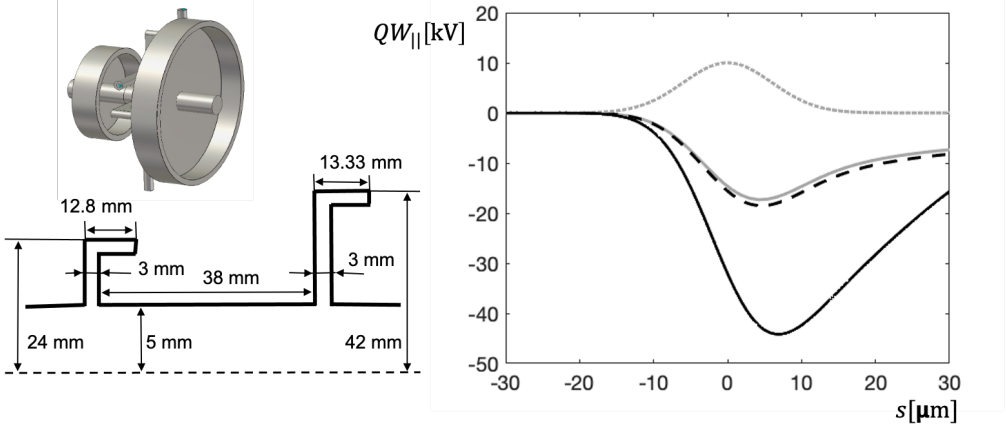

Figure 6: The left picture shows the geometry of BPM. The curves in the right plot present the geometrical and the total wake potentials of BPM for the Gaussian bunch with rms width $\sigma = 5.98$ μm (dotted gray line) as described in the text.

The BPM in the undulator intersection shown in Fig. 6 consists of two cavities with the gap length $g = 3$ mm each. For the short electron bunches with rms length $\sigma << a$ the geometrical part of the wake function can be approximated by expression [17]

$$w_{\parallel}(s) = 2w_{\parallel}^{d}(s), \tag{29}$$

$$w_{\parallel}^{d}(s) = \frac{cZ_0}{\pi^2 a}\sqrt{\frac{g}{2s}}, \tag{30}$$

where factor 2 in Eq. (29) is due to two cavities available in the BPM. The contribution of the material properties of the pipe of BPM is taken into account analytically with help of Eq. (3).

In Fig. 6 the solid gray line presents the geometrical wake potential for the Gaussian bunch with rms length $\sigma = 5.98$ μm calculated with code ECHO [16]. The dashed black line is the analytical approximation from Eq. (29). The solid black line shows the total wake potential which is the direct sum of the analytically obtained geometrical wake potential and the one obtained for the wall properties by Eq. (3).

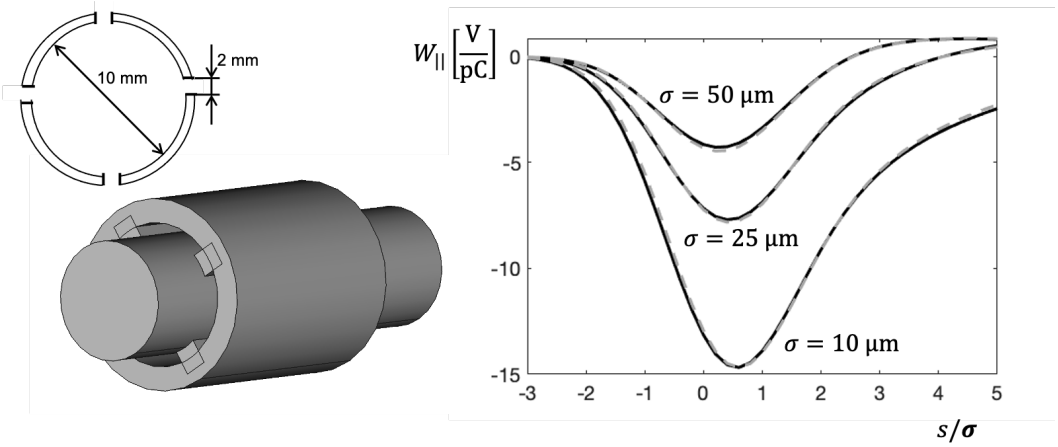

Figure 7: The left picture shows the geometry of the vacuum region with the pumping slots. The solid curves in the right plot present the geometrical wake potentials of the slots for the Gaussian bunch with rms width σ =10, 25, 50 μm obtained numerically. The gray dashed curves are obtained from the analytical approximation by Eq. (31).

The round pipe in the intersection has 4 pumping slots of length $g = 21$ mm and width $w = 2$ mm. The thickness of the pipe at the pump region is 1 mm. The left picture in Fig. 7 shows the geometry of the vacuum volume used in the numerical simulations with code ECHO. We have done the simulations for the perfectly conducting geometry for the Gaussian bunches with rms length of 10, 25 and 50 micrometers. The obtained wake potentials are shown by solid black lines in Fig. 7. From the numerical fitting procedure we have found that these wake potentials can be reconstructed from wake function of the following form

$$w_{\parallel}(s) = 0.85\frac{\theta}{2\pi}w_{\parallel}^{d}(s) + 2.3\frac{cZ_0}{\pi^2 a}\cos\left(\frac{s}{s_0}\right)^{0.175}, \quad \theta = 8\sin^{-1}\left(\frac{w}{2a}\right), \tag{31}$$

where $s_0 = 0.12$ μm is the fit parameter and $\theta/(2\pi)$ is the fraction of the circumfer-

ence occupied by the slots. The gray dashed curves in Fig. 7 present the analytical approximation of the wake potential obtained with help of Eq. (31).

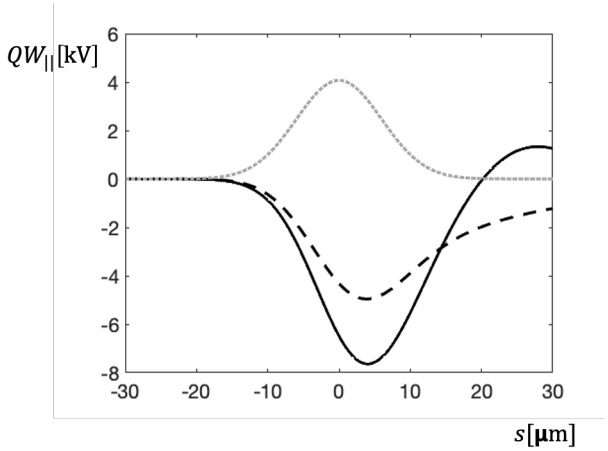

Figure 8: The dashed black line presents the geometrical wake potential of the pumping slots for the Gaussian bunch with rms length $\sigma = 5.98\,\mu$m from the analytical approximation of Eq. (31). The solid black line shows the total wake potential which is the direct sum the geometrical wake potential and the one obtained for the wall properties.

The wake of the pipe between the pumping slots due to the wall material properties is estimated as the steady state wake of the round pipe, Eq. (3), multiplied by material filling factor $1 - \theta/(2\pi)$.

In Fig. 8 the dashed black line presents the geometrical wake potential for the Gaussian bunch with rms length $\sigma = 5.98\,\mu$m for the analytical wake function approximation, Eq. (31). The solid black line shows the total wake potential which is the direct sum of the analytically obtained geometrical wake potential and the one obtained for the wall properties as described above.

The gaskets and the weldseams listed in Table 1 can be considered as short gaps and the wake functions of these elements can be estimated by diffraction model, Eq. (30). For the elements in the elliptical pipe we use Eq. (30) with radius $a = g(F_{||}^{ellip})^{-0.5} = 5.2$ mm. For the Gaussian bunch of rms length σ the loss factor and the energy spread of

the wake potential at the diffraction model can be found as

$$k_{\parallel} = \frac{Z_0 c}{4a\pi^{2.5}}\Gamma\left(\frac{1}{4}\right)\sqrt{\frac{g}{\sigma}}, \quad k_{\parallel,rms} = 0.4k_{\parallel}, \tag{32}$$

where Γ is the gamma function.

4. Impedance budget and the wake function of the undulator lines

In the following we neglect the interference between the wake fields of different elements and suggest that that the total wake function of one undulator section of length $L = 6.1$ m can be well approximated by direct sum of the wake functions of all elements listed in Table 1. The total energy loss of the electron bunch is the direct sum of the energy losses caused by individual elements. For the Gaussian bunch with charge of 250 pC compressed to the peak current of 5 kA the impedance budget of one section with the contribution of all elements is shown in Table 4.

In order to figure out an analytical form of the longitudinal wake function we have combined and modified different analytical approximations for the short range wake functions which can be found at [18, 19, 20]. From numerical experiments we have found that the longitudinal wake function can be accurately approximated by the analytical expression

$$w_{\parallel}(s) = w_0(s) + \frac{\partial}{\partial s}w_1(s) + c\frac{R}{L}\delta(s), \tag{33}$$

$$w_0(s) = A\frac{Z_0 c}{\pi a^2}\exp\left(-\frac{s}{s_0}\right)^{\alpha}\cos\left(\frac{s}{s_1}\right), \tag{34}$$

$$w_1(s) = \frac{Z_0 c}{L\pi^2 a}\sqrt{2g_0 s}, \tag{35}$$

where $A = 1.03$, $a = 5$ mm, $\alpha = 1.3$, $s_0 = 34$ μm, $s_1 = 9.7$ μm, $g_0 = 123$ mm, $R = 30.5$ Ohm. Here parameters g_0 and R can be straightforwardly obtained from the previous calculations and the parameters A, s_0, s_1, α are obtained by a numerical fit of the parametric form of function w_0 to the direct sum of the wakes of different elements listed in Table 1. The term $w_0(s)$ is a modified resonance approximation of the short-range resistive wake function of a round pipe [18].

The dashed black curve in the left plot of Fig. 9 shows the analytical approximation by Eq. (34) of the first term in Eq. (33). The same term obtained from the direct sum

Table 4: Impedance budget of one undulator section with length of 6.1 m for the Gaussian bunch with charge of 250 pC compressed to the peak current of 5 kA

N	Name	Positions	Total length	Loss	Spread
			mm	kV	kV
1	Elliptical pipe	5	5426.7	584.0	275.5
2	Round pipe	12, 14, 16, 20, 22	446.5	110.9	53.7
3	Absorber	11	3.0	71.2	28.0
4	Round/elliptical transition	23	8.0	37.1	14.6
5	BPM	18	99.0	28.7	13.4
6	Below gaps	13, 21	5.0	12.0	4.8
7	Elliptical gaskets	1, 9	1.0	5.1	2.1
8	Round gaskets	17, 19	1.0	5.4	2.2
9	Pumping slots	15	21.0	5.3	2.2
10	Flanges, type I	2, 8	26.0	3.8	2.1
11	Flanges, type II	3, 7	25.1	2.7	1.3
12	Flange, type III	10	27.5	3.0	1.4
13	Weldseams	4, 6	0.2	2.3	0.9
	Totally		6100	871.4	381.4

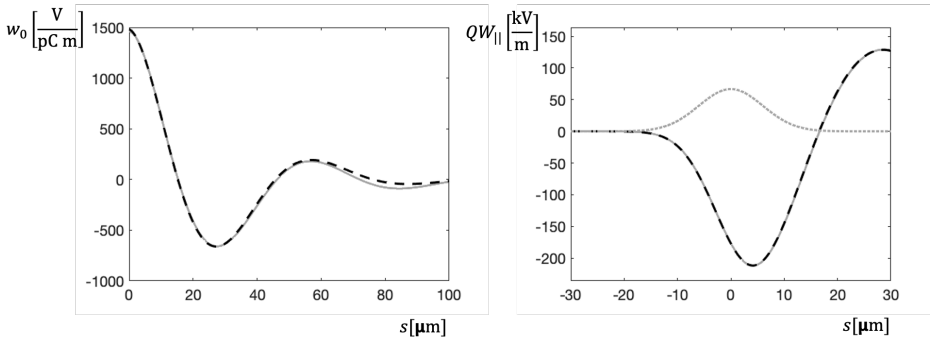

Figure 9: The dashed black curve in the left plot shows the analytical approximation by Eq. (34) of the first term in Eq. (33). The same term obtained from the direct sum is shown by solid gray line. The right plot compares the analytically obtained wake potential (dashed black curve) with the total wake potential (solid gray curve) for the Gaussian bunch (dotted gray line) with charge of 250 pC compressed to the peak current of 5 kA.

of the wake functions of individual components is shown by solid gray line and the agreement is reasonable.

The right plot in Fig. 9 compares the analytically obtained wake potential (dashed black curve) with the total wake potential (solid gray curve) for the Gaussian bunch (dotted gray line) with charge of 250 pC compressed to the peak current of 5 kA. The total wake potential is obtained as direct sum of the wake potentials of individual components listed in Table 1.

5. Optimal linear taper

The knowledge of the wake function allows to calculate the optimal linear undulator tapering for a known bunch shape. For the Gaussian bunch with the charge of 250 pC and the peak current of 5 kA the loss at the peak current position is $W_{\parallel}(0) = 177$ kV/m.

Due to the incoherent synchrotron radiation (ISR) and the wake fields the electrons at the peak current position lose in the undulator the energy

$$\left[\frac{d\gamma(z)}{dz}\right]_u = -\frac{3}{2} r_e \gamma^2 K^2 k_u^2 + \frac{e}{m_e c^2} W_{\parallel}(0), \quad k_u = \frac{2\pi}{\lambda_u}, \quad r_e = \frac{e^2}{m_e c^2 4\pi\epsilon_0}, \tag{36}$$

where K is the undulator parameter, λ_u is the undulator period, ϵ_0 is the permittivity of vacuum, e and m_e are the charge and the mass of the electron.

The normalized linear part of the detuning parameter $C(z) = k_u - k(1 + K^2)/(2\gamma^2)$ reads

$$b_1(z) = \left(\frac{\lambda_u}{4\pi\rho}\right)^2 \frac{d}{dz} C(z) = -\frac{\lambda_u}{4\pi\rho^2} \left(\frac{K(0)}{1 + K(0)^2} \frac{dK(z)}{dz} - \frac{1}{\gamma(0)} \frac{d\gamma(z)}{dz}\right), \tag{37}$$

where ρ is the Pierce parameter [21].

Additionally to the losses in the undulator we have the losses due to the wake fields in the intersections. We have to compensate these losses by an additional tapering in the undulator. Hence we have to use in Eq.(37) a modified term

$$\frac{d\gamma(z)}{dz} = \left[\frac{d\gamma(z)}{dz}\right]_u + \frac{L - L_u}{L_u} \frac{e}{m_e c^2} W_{\parallel}(0), \tag{38}$$

where $L = 6.1$ m and $L_u = 5$ m. The last expression does not include the losses due to coherent synchrotron radiation (CSR) which are considerable near the saturation.

In order to keep the resonance condition, $b_1 = 0$, the taper has to compensate the energy loss

$$\frac{dK(z)}{dz} = \frac{1 + K(0)^2}{K(0)\gamma(0)} \frac{d\gamma(z)}{dz}. \tag{39}$$

It is shown in [21] (see Fig. 2 in [21]) that the mild positive tapering

$$\frac{dK(z)}{dz} = \frac{1 + K(0)^2}{K(0)} \left(\frac{1}{\gamma(0)} \frac{d\gamma(z)}{dz} - b_1 \frac{4\pi\rho^2}{\lambda_u} \right). \tag{40}$$

with $b_1 < 0.25$ increases the power at saturation compared with a pure energy loss compensation of Eq.(39).

Table 5: Parameters at the SASE1 undulator line

Parameter	Value	Units
Photon beam energy	9.3	keV
Electron beam energy	14	GeV
Slice energy spread	2.2	MeV
Electron beam emittance	0.5	μm
Beam charge	250	pC
Peak current	5	kA
Averaged optical β-function	32	m
Undulator period	4	cm

As an example we consider the optimal taper for the parameters of the electron beam and the radiation at the SASE1 undulator line listed in Table 5. In order to find the optimal taper we have done numerical simulations of free electron laser physics with code ALICE [22]. Initially we do a fast two dimensional scan: for tapering parameter dK/dz in the range from 0 to 15e-4 1/m we look for the optimal initial detuning $C(0)$ which gives the highest growth rate of the radiation in the linear regime. The scan has been done in the amplifier model for only one slice with the power of the initial field equivalent to the shot noise power of the electrons in the beam [23]. The black solid curve in the left plot in Fig. 10 shows the power obtained for the optimal initial detuning parameter $C(0)$ at the saturation distance for different values of tapering dK/dz or, equivalently, for different values of the normalized linear part of the detuning

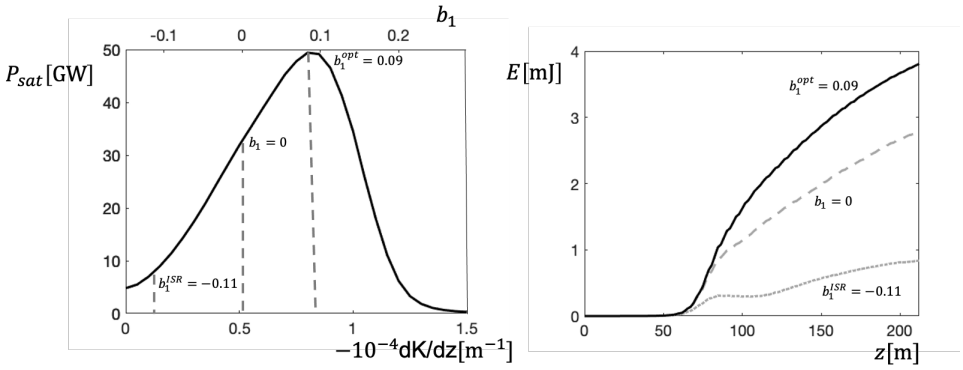

Figure 10: The black solid curve in the left plot shows the radiation power at the saturation for the optimal initial detuning parameter. The three vertical dashed gray lines show three different taperings: the one that compensates only the losses to ISR, the one that additionally compensates the losses due to the wake fields, the one that corresponds to the optimal linear taper. The radiation energy in the SASE pulse along the undulator for these three cases is shown in the right plot.

b_1. The three vertical dashed gray lines shows three different taperings: the one that compensates only the losses to ISR, $b_1^{ISR} = -0.11$, the one that additionally compensates the losses due to the wake fields , $b_1 = 0$, and the one that corresponds to the optimal linear taper, $b_1^{opt} = 0.09$. The radiation energy in the SASE pulse alongh the undulator for these three cases is shown in the right plot in Fig. 10. The simulations are done at the SASE model which includes incoherent radiation, quantum fluctuations and the correct modeling of the intersections. As expected an overcompensation of the losses due to the ISR and the wake fields with $b_1^{opt} = 0.09$ allows to obtain a higher energy of the radiation at the saturation distance. This overcompensation allows partially to compensate the losses due to CSR near the saturation. A better compensation of the losses due to CSR radiation near the saturation and after it can be obtained with non-linear tapering [24].

6. Discussion

The wake functions of different components of the undulator lines are calculated separately and the total wake function is obtained as a direct sum of the individual contributions. However, for the bunches much shorter than the pipe radius there must

be significant impedance coupling between the components which are close to each other.

In order to investigate this question, we have created a rotationally symmetric model of the undulator vacuum chamber. The elliptical undulator pipe and other elements with the elliptical cross-section listed in Table 1 have been replaced by round elements with an "equivalent" radius

$$a = \frac{g}{\sqrt{F_{\parallel}^{ellip}\left(\frac{g}{w}\right)}}, \tag{41}$$

where w is the half-width and g is the half-height of the elliptical cross-section. We have neglected the roughness and the oxide layer effects. Additionally we have considered only DC conductivity model (Eq. (4) with $\tau = 0$). The pumping slots are replaced by round pipe of the radius of 5 mm.

For this "round" model we have calculated the longitudinal wake function in the same way as described in this paper. The energy loss $U(z)$ due to this model increases uniformly along the undulator section and its change $\Delta U(\Delta z)$ relative to the beginning of the undulator section can be written as

$$\Delta U(\Delta z) = e k_{\parallel} \Delta z,$$

where Δz is the position in the undulator section relative to the beginning of the section, e is the charge of electron, $k_{\parallel}$ is the "analytical" loss factor (per meter).

Alternatively, we have done direct numerical calculations with time-domain code ECHO [16]. Here we have started from the perfectly conducting pipe and considered 3 undulator sections with the total length of 18.3 m. The Gaussian bunch is traveling on the axis and we have calculated the energy loss of the bunch along the undulator line:

$$U(z) = -e\int_{-\infty}^{\infty} W_{\parallel}(s,z)\lambda(s)ds, \quad W_{\parallel}(s,z) = -\frac{1}{Q}\int_{-\infty}^{z-s} E_z\left(z', t = \frac{z'+s}{c}\right)dz'.$$

The comparison of the "analytical" energy loss with the one obtained from the numerical calculations is shown in Fig. 11. The left plot shows the results for the rms bunch length σ of 50 μm. The solid black line presents the grow of the energy loss along one middle undulator section. The dotted black line describes the energy loss

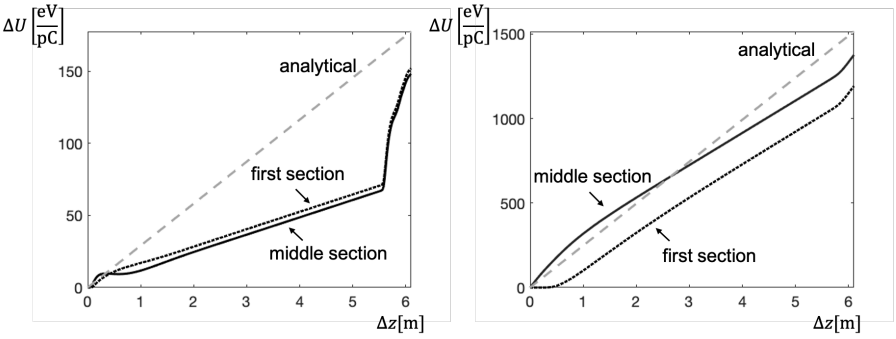

Figure 11: The comparison of the "analytical" energy loss with the energy loss obtained from the numerical calculations with code ECHO for rotationally symmetric geometry. The left plot shows the results for the bunch length of 50 μm. The right plot shows the results for the bunch length of 10 μm. The solid black lines present the grow of the energy loss along one middle undulator section. The dotted black lines describe the energy loss grow in the first undulator section. The gray dashed lines present the "analytical" energy loss.

grow in the first undulator section. The curves are different due to transitive effects at the beginning of the undulator line. The gray dashed curve presents the "analytical" energy loss. The similar results for the much shorter bunch length of 10 μm are shown at the right plot of Fig. 11.

If we define the "interference" factor $F_{int}(\sigma)$ as a ratio of the numerical energy loss at the end of middle section to the "analytical" energy loss of one section then we can write $F_{int}(50\ \mu m) = 0.84$, $F_{int}(10\ \mu m) = 0.91$. Such behavior of the interference factor can be explained by smaller contribution of "geometrical" wake relative to the contribution of the resistive wake for the shorter bunch length.

For the Gaussian bunch of length $\sigma = 10\ \mu$m the catch-up distance [19] in the pipe of radius $a = 5$ mm can be estimated as $\sigma^2/a = 2.5$ m. Indeed, we see at the right plot of Fig. 11 that the black solid curve demonstrates the steady-state behavior only after 2 meters from the beginning of the elliptical pipe.

Nevertheless, the catch-up distance does not impact the choice of the optimal undulator taper because the loss factor of middle undulator section is independent from the catch-up distance. Additionally, the transitive behavior in the first undulator section is suppressed in the real setup of the machine due to the vacuum pipe radius reduction from 20.25 mm to 5 mm at the distance of approximately 0.7 m before the undulator

entrance.

7. Summary

From the numerical simulations and the theoretical estimations we have found analytical approximations of the longitudinal wake functions of individual components present at the undulator lines of the European x-ray free electron laser. It has allowed us to derive a simple form of an analytical approximation of the short-range longitudinal wake function of undulator lines. A choice of the optimal linear undulator taper for a known wake function was discussed on the example of the parameters of SASE1 undulator line. Additionally, we have presented a numerical algorithm to estimate the impedance of arbitrary shaped pipes with known surface impedance.

Declaration of competing interest

The authors declare that they have no known competing financial interests or personal relationships that could have appeared to influence the work reported in this paper.

Appendix A. Approximate boundary conditions

The surface impedance boundary condition between the tangential components of the electric field $\boldsymbol{E}$ and the magnetic field $\boldsymbol{H}$ reads

$$\boldsymbol{n} \times \boldsymbol{E} = Z_s \boldsymbol{n} \times \boldsymbol{n} \times \boldsymbol{H},$$

where $\boldsymbol{n}$ is the vector normal to the pipe surface ∂S. It reduces to the relations

$$E_z = -Z_s H_t, \qquad E_t = Z_s H_z,$$

where E_t and H_t are the components of the electric and magnetic fields tangential to the pipe surface ∂S. In order to exclude the magnetic field from the first equation let us

to consider the Maxwell equations in the component form for relativistic bunch with current density $J_z = j_z e^{i(\omega t - kz)}$, $\omega = kc$,

$$\partial_y E_z + ikE_y = -ikZ_0 H_x, \qquad \partial_y H_z + ikH_y = ikZ_0^{-1} E_x,$$
$$\partial_x E_z + ikE_x = ikZ_0 H_y, \qquad \partial_x H_z + ikH_x = -ikZ_0^{-1} E_y,$$
$$\partial_x E_y - \partial_y Ex = -ikZ_0 H_z, \qquad \partial_x H_y - \partial_y H_x = -ikZ_0^{-1} E_z + j_z.$$

where Z_0 is the free space impedance. The tangential component of the magnetic field $\boldsymbol{H}_\perp$ can be written as

$$H_t = n_x H_y - n_y H_x = n_x \left(\frac{1}{Z_0} E_x + \frac{1}{ikZ_0} \partial_x E_z \right) + n_y \left(\frac{1}{Z_0} E_y + \frac{1}{ikZ_0} \partial_y E_z \right) =$$
$$\frac{1}{Z_0} E_n + \frac{1}{ikZ_0} \left(n_x \partial_x E_z + n_y \partial_y E_z \right) = \frac{1}{Z_0} E_n + \frac{1}{ikZ_0} \partial_{\boldsymbol{n}} E_z.$$

Hence the impedance boundary condition can be rewritten as

$$E_z = \frac{Z_s}{Z_0} \left(E_n + \frac{1}{ik} \partial_{\boldsymbol{n}} E_z \right), \quad E_t = \frac{Z_s}{ik} \boldsymbol{\nabla}_\perp \boldsymbol{H}_\perp,$$

where we have used Eq. (8). In the high-frequency approximation, $k >> 1$, these equations can be simplified to the form

$$E_z = \frac{Z_s}{Z_0} E_n, \quad E_t = 0.$$

Appendix B. Longitudinal form factors of elliptical and round wave-guides

It is well known [7, 25] that the longitudinal wake function of round pipe of radius g with a retardation layer has the following value at the origin

$$w_\parallel^{round}(0) = \frac{Z_0 c}{2\pi g^2}, \quad w_\parallel^{round}(0+) = 2 w_\parallel^{round}(0)$$

where "0+" means the one-sided limit from the right.

An ellipse with semi-major axis w and semi-minor axis g can be conformally mapped onto the circle of radius g by transformation [26]

$$f^{ellip}(z) = g\sqrt{k}\, \mathrm{sn}\left(\frac{2K}{\pi} \arcsin\left(\frac{z}{\sqrt{(w^2 - g^2)}} \right), k^2 \right),$$

where sn is the Jacobi elliptic sine function and

$$k = \left(\frac{\theta_2(0,p)}{\theta_3(0,p)}\right)^2, \quad K = \frac{\pi}{2}\theta_3^2(0,p), \quad p = \left(\frac{w-g}{w+g}\right)^2.$$

Here θ_2, θ_3 are Jacobi theta functions. Following [25] we can write the value of the longitudinal wake function of the elliptical wave-guide at the origin as

$$w_\parallel^{ellip}(0) = w_\parallel^{round}(0) F_\parallel^{ellip}\left(\frac{g}{w}\right), \quad F_\parallel^{ellip}\left(\frac{g}{w}\right) = \left(\frac{d}{dz} f^{ellip}[0]\right)^2 = \left(\frac{g}{w}\right)^2 \frac{4kK^2}{\pi^2(1-(g/w)^2)},$$

where $F_\parallel^{ellip}$ is the longitudinal form factor of the elliptical wave-guide.

A rectangle with width $2w$ and height $2g$ can be conformally mapped onto the circle of radius g by transformation [27]

$$f^{rect}(z) = g\frac{1 + i\sqrt{k}\,\mathrm{sn}(Kw^{-1}(z+ig))}{i + \sqrt{k}\,\mathrm{sn}(Kw^{-1}(z+ig))},$$

where the symbols K and k have the same meaning as for the ellipse above but the value of p is different:

$$p = e^{-2\pi g/w}.$$

Hence the longitudinal wake function of the rectangular wave-guide at the origin can be written as

$$w_\parallel^{rect}(0) = w_\parallel^{round}(0) F_\parallel^{rect}\left(\frac{g}{w}\right),$$
$$F_\parallel^{rect}\left(\frac{g}{w}\right) = \left(\frac{d}{dz} f^{rect}[0]\right)^2 = \left(\frac{g}{w}\right)^2 \frac{4kK^2\left(\mathrm{cn}(iK\frac{g}{w}, k^2)\,\mathrm{dn}(iK\frac{g}{w}, k^2)\right)^2}{\left(i + \sqrt{k}\,\mathrm{sn}(iK\frac{g}{w}, k^2)\right)^4},$$

where sn, cn, dn are elliptic Jacobi functions and $F_\parallel^{rect}$ is the longitudinal form factor of the rectangular wave-guide.

The form factors allow simple cubic approximations:

$$F_\parallel^{ellip}(x) = 0.279x^3 + 0.093x^2 + 0.013x + \pi^2/16,$$
$$F_\parallel^{rect}(x) = 0.477x^3 - 0.268x^2 + 0.036x + \pi^2/16, \quad x = g/w, \quad g \le w,$$

with maximal absolute error below 0.3%.

References

[1] B.W. Zotter, S.A. Kheifets, Impedances and Wakes in High-Energy Particle Accelerators, World Scientific, Singapore, 1998.

[2] W. Decking et al, A MHz-repetition-rate hard X-ray free-electron laser driven by a superconducting linear accelerator, Nat. Photonics 14 (2020) 391.

[3] N.W. Ashroft, N.D. Mermin, Solid State Physics, Harcourt College Publishers, USA, 1976.

[4] K.L.F. Bane and G. Stupakov, Resistive Wall Wake Field in the LCLS Undulator Beam Pipe, SLAC-PUB 10707, SLAC, 2004.

[5] A. Tsakanian, M. Dohlus, I. Zagorodnov, The Effect of the Metal Oxidation on the Vacuum Chamber Impedance, TESLA-FEL 2009-05, DESY, 2009.

[6] M. Dohlus, Impedance of Beam Pipes with Smooth Corrugations, TESLA 2001-26, DESY, 2001

[7] K. Bane, G. Stupakov, Using surface impedance for calculating wake fields in flat geometry, Phys. Rev. ST Accel. Beams 18 (2015) 034401.

[8] A. Lutman, R. Vescovo, P. Craievich, Electromagnetic field and short-range wake function in a beam pipe of elliptical cross section, Phys. Rev. ST Accel. Beams 11 (2008) 074401.

[9] K. Yokoya, Resistive wall impedance of beam pipes of general cross section, Part. Accel. 41 (1993) 221.

[10] A. Doicu, Y.A. Eremin, T. Wriedt, Acoustic and Electromagnetic Scattering Analysis Using Discrete Sources, Academic Press, London, 2000.

[11] A.W. Chao, Physics of Collective Beam Instabilities in High Energy Accelerators, Wiley, New York, 1993.

[12] G. Stupakov, K. L. F. Bane, I. Zagorodnov, Optical approximation in the theory of geometric impedance, Phys. Rev. ST Accel. Beams 10 (2007) 054401.

[13] R. Gluckstern, J. Van Zeijts, and B. Zotter, Coupling impedance of beam pipes of general cross section, Phys. Rev. E 47 (1993) 656.

[14] S. A. Heifets, On the Directional Symmetry of the Impedance, SLAC/AP-79, SLAC, 1990.

[15] I. Zagorodnov, Indirect methods for wake potential integration, Phys. Rev. ST Accel. Beams 9 (2006) 102002.

[16] I. Zagorodnov, T. Weiland, TE/TM field solver for particle beam simulations without numerical cherenkov radiation, Phys. Rev. ST Accel. Beams 8 (2005) 042001.

[17] K. Bane and M. Sands, Wakefields of Very Short Bunches in an Accelerator Cavity, SLAC-PUB 4441, SLAC, 1987.

[18] K.L.F. Bane and M. Sands, The Short-Range Resistive Wall Wakefields, SLAC-PUB-95-7074, SLAC, 1995.

[19] K.L.F.Bane, Wakefields of sub-picosecond bunches, SLAC-PUB-11829, SLAC, 2006.

[20] I. Zagorodnov, Analytical impedance models for very short bunches, in: Proceedings of ICFA Mini-Workshop on Impedances and Beam Instabilities in Particle Accelerators,Italy, 18-22 September 2017, CERN Yellow Reports, CERN, Geneva, vol.1, 2018, p. 133.

[21] E.L.Saldin, E.A. Schneidmiller, M.V. Yurkov, Self-amplified spontaneous emission FEL with energy-chirped electron beam and its application for generation of attosecond x-ray pulses, Phys. Rev. ST Accel. Beams 9 (2006) 050702.

[22] I. Zagorodnov, Numerical modeling of collective effects in free electron lasers, in: Proceedings of the 2010 International Computational Accelerator Physics Conference, Rostock-Warnemuende, Germany, 2012, p.81.

[23] E.L. Saldin, E.A. Schneidmiler, M.V. Yurkov, The Physics of Free Electron Lasers, Springer-Verlag, Berlin, Heidelberg, 2000.

[24] E.A. Schneidmiller, M.V. Yurkov, Optimization of a high efficiency free electron laser amplifier, Phys. Rev. ST Accel. Beams 18 (2015) 030705.

[25] S.S. Baturin, A.D. Kanareykin, New method of calculating the wakefields of a point charge in a waveguide of arbitrary cross section, Phys. Rev. Accel. Beams 19 (2016) 051001.

[26] G. Szego, Conformal mapping of the interior of an ellipse onto a circle, The American Mathematical Monthly 57 (1950) 474.

[27] A.B. Schubert, Conformal Mapping of a Circle onto a Rectangle, BNWL-901, Battelle-Northwest, Richland, Wash. Pacific Northwest Lab., 1968.